

Monte Carlo Calculation of the Single-Particle Spin-Echo Small-Angle Neutron Scattering Correlation Function

Hakon Kaya

Department of Chemical Engineering, University of Amsterdam,
Nieuwe Achtergracht 166, 1018 W V Amsterdam, The Netherlands.
hkaya@ulb.ac.be

April 17, 2024

Abstract

A Monte Carlo algorithm for calculating the single-particle spin-echo small-angle neutron scattering (SESANS) correlation function is presented. It is argued that the algorithm provides a general and efficient way of calculating SESANS data for any given shape and structure.

PACS 61.12.Ex, 02.70.Tt, 07.05.Kf, 02.50.Ng

1 Introduction

Spin-echo small-angle neutron scattering (SESANS) has recently emerged as a new way of applying neutron scattering to the investigation of the structure of matter [?, ?]. The method is particularly useful for large structures in the size range from 10 nm up to several microns. This is the same size range covered by techniques like light scattering and ultra-small angle neutron scattering (USANS). The use of neutron spin echo in measuring elastic scattering, however, renders beam collimation unnecessary, thus avoiding the low fluxes from which USANS suffers. In comparison to light scattering, the use of neutron allows for study of opaque or highly concentrated samples. The SESANS method is presently on an active developing stage, and the theoretical concepts and methods from which conventional small-angle neutron scattering (SANS) benefits have only recently started to be derived [?] and be applied to the analysis of experimental data [?]. As in the case of SANS, the data analysis can be performed with model-dependent or model-independent methods. In the latter case, the experimentally obtained scattering functions are inverted to obtain a curve representing the pair distance distribution function $p(r)$. The most well-known realisation for this procedure is the Indirect Fourier Transform by Glatter [?]. Similar analysis can be carried out by the maximum entropy method [?] and the regularization method of Svergun [?]. Model-independent analysis is particularly simple in the case of SESANS, as the relation between the SESANS correlation function $G(z)$ and the small-angle scattering correlation function $\chi(r)$ is given by an Abel integral equation [?], for which there exist standard numerical methods for solution.

In model-dependent analysis, mathematical functions that model the scattering intensity from a system of particles with presumed shape, structure, and ordering are fitted to the experimental data. From the fitted parameters one obtains information such as the size and shape of the particles, their inner structure and size distribution, and the inter-particle interactions that create ordered structures. In SANS terminology, the last piece of information is contained in the structure factor, whereas information pertaining to single-particle scattering is contained in the form factor. Analytical or semi-analytical functions for the scattering form factors or scattering amplitudes are known for several geometries [?]. These functions are easy to extend to include core-shell structures and polydisperse assemblies.

As will be elaborated in the following section, $G(z)$ is related to the SANS scattering cross section $d\sigma/d\Omega = (d)$ by a two-dimensional cosine transform [?]. Knowing the full detectable $d\sigma/d\Omega = (d)$ as an analytical function or as tabulated values of (d) vs. Q , calculation of $G(z)$ is straightforward by numerical integration. In principle, it would be desirable and more efficient with analytical expressions for $G(z)$ for different geometries, analogous to form factors for SANS, so that SESANS data can be analyzed with a similar toolbox of model functions. Analytical expressions for $G(z)$ for scattering from single homogeneous and hollow spheres have already been derived using the concept of the mass correlation function $\chi(r)$ [?]. If $\chi(r)$ of a given structure is known, calculation of $G(z)$ is

simple. For non-spherical geometries, however, expressions for $\rho(r)$ can take complicated forms [?, ?, ?]. Moreover, it is not an easy task to extend $\rho(r)$ from homogenous to multi-domain structures.

In this paper we investigate an alternative method to calculate $G(z)$. It is for all practical purposes of general validity and straightforward to implement for any shape and structure. The idea is to perform a Monte Carlo calculation of the pair distance distribution function $p(r)$, from which the SESANS correlation function $G(z)$ and also the SANS scattering cross section $(d)=(d)$ can be calculated by a single numerical integration. Monte Carlo methods have been used by several authors in calculation of SANS spectra [?, ?, ?, ?]. The algorithm for calculating SESANS curves is outlined in Section 3. In Section 4 we present results of the calculations for different shapes and structures.

2 SESANS Theory

The measured quantity in a SESANS experiment is the loss of polarization a neutron beam suffers by being scattered by the sample. By passing through magnetic fields before and after interacting with the sample, the neutrons are subjected to Larmor spin precession. In the case of no interaction with the sample, the precessions before and after the sample area cancel each other, yielding a spin echo preserving the polarization state of the beam [?]. The presence of a scattering sample produces precession length differences that are functions of the scattering angle. The ensuing depolarization is a function of the SESANS correlation function $G(z)$ [?]:

$$\frac{P(z)}{P_0} = \exp[G(z) - G(0)] = \exp[G(0)(G_0(z) - 1)]; \quad (1)$$

where $G_0(z)$ is the normalized correlation function. The relation between the SANS macroscopic scattering cross section $(d)=(d)$ and the SESANS correlation function has already been derived [?, ?]:

$$G(z) = \frac{t^2}{4} \int_{-1}^1 \int_{-1}^1 (d)_y (d)_z \frac{(d)(Q)}{(d)} \cos(Q_z z); \quad (2)$$

where λ and t denote the wavelength of the neutron beam and the thickness of the sample, respectively. Q_y and Q_z are the cartesian components of the scattering vector Q , the incident beam lying along the x axis. The integrations in (2) are in practice defined by the area in the yz -plane covered by the detector. The spin-echo length z is a function of the neutron wavelength, the sample position, and the configuration of the magnetic fields [?].

We now consider a system of non-interacting particles isotropically embedded in a homogenous matrix or dispersed a solvent. The SANS scattering cross section can be written in terms of an intra-particle form factor $P(Q)$ and an inter-particle structure factor $S(Q)$:

$$\frac{(d)}{(d)}(Q) = n_p V^2 P(Q) S^0(Q); \quad (3)$$

where n_p is the number density of scattering particles and V is the volume of a particle. Most of the analytical structure factors have been calculated for systems of monodisperse spheres. The effective structure factor $S^0(Q)$ includes approximate corrections to $S(Q)$ due to particle polydispersity or anisotropy [?, ?, ?]. We will in the following consider dilute system, for which we may ignore inter-particle scattering and set $S^0(Q) = 1$, corresponding to an ideal gas. The form factor $P(Q)$ is related to the average size and shape of the individual particles and to their inner structure. Focusing on a single particle, the form factor can be written in terms of the density correlation function $\gamma(r)$:

$$P(Q) = \int_0^{Z_D} \gamma(r) \frac{\sin Qr}{Qr} 4\pi r^2 dr; \quad (4)$$

where $\gamma(r)$ is defined by [?, ?]:

$$\gamma(r) = \frac{1}{V} \int_V \langle \rho(\mathbf{d}) \rho^0(\mathbf{r}^0 + \mathbf{r}) \rangle; \quad (5)$$

where the braces $\langle \rangle$ denote averaging over all orientations of the position vector \mathbf{r} . $\rho(\mathbf{r})$ is the scattering length density at a position \mathbf{r} inside the particle, minus the constant scattering length of the surrounding medium (in most cases a solvent). D is the largest chord length of the particle, so that $\gamma(r) = 0$ for $r > D$. For a homogenous particle $\gamma(r)$ is proportional to the overlap volume between the particle and its identical "ghost" that has been shifted by a distance \mathbf{r} . For an inhomogenous particle, the volume of the overlapping region must be weighted with the product of the scattering length densities of the respective regions [?]. An important identity is [?]:

$$\langle \gamma \rangle^2 V = \int_0^{Z_D} \gamma(r) 4\pi r^2 dr; \quad (6)$$

where $\langle \gamma \rangle$ is the difference between the average scattering length density of the particle and that of the surrounding medium (in most cases a solvent). The normalized density autocorrelation function $\gamma_0(r)$ is defined through $\gamma(r) = \langle \gamma \rangle^2 \gamma_0(r)$ and has the property $\gamma_0(0) = 1$.

In this paper we focus on the single-particle contribution to the SESANS spectrum. A direct real-space interpretation of $G(z)$ was presented by Kruglov et al. in 2003. For a system of non-interacting particles, the SESANS correlation function can be written $G(z) = \langle \gamma \rangle^2 n_p G_p(z)$, where the single-particle SESANS correlation function bears the following relation to the structure function $\gamma(r)$:

$$\begin{aligned} G_p(z) &= \frac{1}{V} \int_0^{Z_D} \int_0^{Z_D} \gamma(\mathbf{d}) \frac{1}{x^2 + z^2} d\mathbf{d} \\ &= \frac{1}{2 \langle \gamma \rangle^2 V} \int_0^{Z_D} \int_0^{Z_D} \gamma(\mathbf{d}) \frac{1}{x^2 + z^2} d\mathbf{d}; \end{aligned} \quad (7)$$

Note that both $G(z)$ and $G_p(z)$ are dimensionless. Knowing $\rho(r)$, the SANS form factor and the single-particle SESANS correlation function can be calculated. An important quantity in SESANS is the total scattering probability, given as $G(0)$ [?, ?]. It relates to the observed depolarization and thus gives an indication on the magnitude and detectability of the SESANS signal. From the above we have:

$$\begin{aligned} G(0) &= \int_0^{Z_D} \int_0^{Z_D} \rho(r) \rho(d) \, dr \, dd \\ &= \int_0^{Z_D} \int_0^{Z_D} \rho(r)^2 \, dr \, dd \\ &= \int_0^{Z_D} \rho(r)^2 \bar{l} \, dr \end{aligned} \quad (8)$$

$$= \int_0^{Z_D} \rho(r)^2 \bar{l} \, dr \quad (9)$$

where $\phi = n_p V$ is the volume fraction of the particles and \bar{l} is the mean length of all chords contained in the particle [?]. Finally in this section, we remark that in the case of an ensemble of polydisperse, non-interacting particles, the equations above take the form

$$G(z) = \int_0^{Z_D} \int_0^{Z_D} \rho(r)^2 V \int_0^{Z_D} \rho(d) \frac{1}{x^2 + z^2} \, dx \, dr \, dd \quad (10)$$

$$G(0) = \int_0^{Z_D} \int_0^{Z_D} \rho(r)^2 V \int_0^{Z_D} \rho(d) \, dx \, dr \, dd; \quad (11)$$

where h_i now stands for the averaging over the particle sizes. The number density is given by $n_p = \phi / V$. If $\rho(r)$ is the same for all particles, Equation (11) can be written $G(0) = \int_0^{Z_D} \rho(r)^2 \bar{l}_w \, dr$, where \bar{l}_w is the weight-averaged mean chord length.

3 Monte Carlo calculation of $G(z)$

3.1 Calculating the pair distance distribution function

The pair correlation function $\rho(r)$ is related to the pair distance distribution function (pddf) $p(r)$ by

$$p(r) = r^2 \rho(r); \quad (12)$$

$p(r)$ is the probability of two random points within the particle being separated by a distance r . By random sampling of distances between points within the particle, and keeping statistics of the sampled distances, $p(r)$ can be found for any particle shape. The interval $0 \leq r \leq D$ is partitioned into $M + 1$ histogram bins, indexed from 0 to M , D being the maximum distance between two points belonging to the particle. $M = 200$ was used for the calculations presented in this paper.

Geometrical points are sampled uniformly from a volume that circumscribes the volume of the given particle as closely as possible. When $N_m = 1000$ points

have been selected, the points that fall outside the shape function of the particle are discarded, leaving N_r points. The points are sampled in batches of N_m in order not to exhaust the computer memory. The shape of the sampling volume is essential, as it ensures that most of the sampled points will belong to the particle. This makes the calculations far more efficient than sampling from a circumscribing rectangular box, discarding the points that fall outside the shape function of the particle [?, ?]. The sampling volumes are rectangular, spherical, or cylindrical, depending on the shape of the particle. Uniform sampling from a given distribution or volume by an inverse method is a well-known technique in Monte Carlo calculations [?]. For completeness, we give a brief outline of the procedure in Appendix A. For the spherical and cylindrical sampling volumes, it is straightforward to limit the sampling to given segments or sectors. Regardless of the shape of the simulation box, it is necessary that it encloses the entire particle ensure that different parts of the particle contribute to $p(r)$ in proportion to their volume. This can also be accomplished by allocating a fraction V_i/V of the randomly selected points to each domain i . This alternative is particularly suited for multidomain structures with inhomogeneous density distributions.

The algorithm proceeds by calculating the $N_r(N_r - 1)/2$ distances defined by the accepted points. The distance $d = |\mathbf{r}_a - \mathbf{r}_b|$ between the points \mathbf{r}_a and \mathbf{r}_b is counted into the histogram, weighted by the product of the scattering length densities ρ_a and ρ_b of the two points. The update of the histogram is carried out by the following algorithm :

$$p(i) \leftarrow p(i) + \int \frac{M d}{D} + 0.5 \rho_a \rho_b; \quad (13)$$

where the $\text{int}()$ function represents truncation of decimals, leaving the integer index i of the histogram bin. The index i is related to the intraparticle distance by $r = iD/M$. Adding 0.5 to the argument of the $\text{int}()$ eliminates the problem overcounting smaller distances because of the decimal truncation.

When the $N_r(N_r - 1)/2$ distances have been counted, the program checks the accuracy of the calculated $p(i)$ after a criterion to be described below. If the accuracy is not accepted, a new batch of N_r points is selected, and the resulting new $N_r(N_r - 1)/2$ distances are counted into the histogram following equation (13). The total number of sampled points belonging to the particle, i.e. accepted points, is denoted N_p ; and the total number of sampled points is denoted N_M .

The normalization of $p(i)$ is done so that the form factor will satisfy $P(Q=0) = 1$. This is accomplished by calculating $p(i) = \tilde{p}(i) / (CD/M)$, where

$$C = \sum_{a=1}^{N_r-1} \sum_{b=a+1}^{N_r} \rho_a \rho_b = \left(\sum_{a=1}^{N_r} \rho_a \right)^2 N_p (N_p - 1)/2 \quad (14)$$

is the sum of the distance weights. The last equality in (14) is valid in the limit of large N_p . For a homogeneous particle, C will be proportional to the number of sampled intra-particle distances. Knowing C , $(\sum \rho_a)^2$ can thus be calculated.

In most cases the volume V of the particle will be known beforehand. If not, it can be found from the MC calculations by the relation $V = N_p V_{\text{box}} / N_M$, where V_{box} is the volume of the simulation box.

Numerical tests showed that a reliable test for the accuracy of $p(i)$ was to compare $p(i)_N$, the pair distance distribution function calculated from N sampled points, with $p(i)_{N=1000}$. This was done for every time $p(i)$ had been calculated with 1000 new points and upgraded with $1000 - (1000 - 1) = 2$ distances. The calculations were halted when

$$\frac{\sum_i [p(i)_N - p(i)_{N=1000}]^2}{\sum_i [p(i)_{N=1000}]^2} < 0.25\% : \quad (15)$$

For homogeneous particles, the required number of points lay around $N_p = 5000$. For inhomogeneous particles, the number could be significantly higher; for core-shell particles with equal volumes and opposite signs of the scattering length densities, values up to $N_p = 40000$ were typical. Nevertheless, calculation of a full data set $G_0(z)$ took only a few seconds on a notebook equipped with a 750 MHz Pentium-III processor.

3.2 Finding $\langle r \rangle$

To find $\langle r \rangle$ from the calculated $p(r)$, Eq. (12) faces us with the problem of dividing by zero or small values of r^2 . We overcome this problem by exploiting the small- r expansion of $\langle r \rangle$:

$$\langle r \rangle = a + br + cr^2 + \dots \quad (16)$$

The expansion parameters are known as differential parameters and are related to structural features of the particle [?]. The second order parameter c will in most cases be zero, and the last term could thus be neglected or replaced with a third-order term dr^3 . For the sake of the generality of the algorithm, however, we apply the expansion as given in equation (16). One should bear in mind, though, that there are particle shapes for which an expansion like (16) can not be carried out [?]. However, it is valid for most realistic geometries. We

find the differential parameters $a; b; c$ by polynomial least-squares fitting [?] of $ar^2 + br^3 + cr^4$ to the Monte Carlo calculated $p(r)$ at small r . For the sum of squared residuals we have:

$$E_m(a; b; c) = \sum_{i=0}^N p_i (ar_i^2 + br_i^3 + cr_i^4)^2; \quad (17)$$

where $r_i = iD/M$. E_m is minimized with respect to a, b , and c ; and the resulting linear system is solved for $a; b; c$ with standard routines [?]. The summation in (17) runs from $i = 0$ to $i = m$, where the index number $m < M$ is decremented until the sum of squared residuals $E_m(a; b)$ has a sufficiently low value. When this is the case, $\langle r \rangle$ up to index $i = m$ is given by $a + br_i + cr_i^2$. For the remaining values of r , $\langle r \rangle$ is calculated directly by $p(r) = r^2$. An example is demonstrated

in Figure 1. In the calculations in this paper, the initial value of m is set at half the distance between $r = 0$ and the first peak of $p(r)$. Finally, to facilitate a consistent computation of $G(z)$ and $G(0)$, $\phi_0(r) = \phi(r)/a$ is calculated by normalization.

3.3 Calculation of $G(0)$ and $G_0(z)$

The single-particle SE SANS correlation function $G_p(z)$ is calculated by numerical evaluation of the integral (7), neglecting the prefactor $2(\frac{1}{2})^2 V$. Having found $\rho_0(x)$, we need to evaluate $\rho_0(\sqrt{x^2 + z^2})$ for arbitrary values of x and z . This is accomplished by natural cubic spline interpolation [?]. The integral (7) is evaluated using a 16-point Gauss-Legendre quadrature [?, ?]. The normalization of $G_p(z)$ is carried out by dividing by $G_p(0)$, which is calculated at the beginning by evaluating (7) for $z = 0$. Subsequent calculations of $G_p(z)$ are normalized by dividing by $G_p(0)$, thus yielding $G_0(z)$. The total scattering probability $G(0)$ is given by $2(\frac{1}{2})^2 n_p^{-2} t G_p(0)$, where the calculation of $(\frac{1}{2})^2$, if unknown a priori, can be done by means of Equation (14).

4 Results and discussion

In Figure 2 we have plotted the MC-calculated $G_0(z)$ curve for a homogenous sphere with radius $R = 50$ together with the analytical expression for $G_0(z)$ [?]. The latter reads:

$$G_0(\lambda) = \frac{1}{2} + \frac{\lambda^2}{8} + \frac{\lambda^4}{24} + \frac{\lambda^6}{720} + \dots; \quad (18)$$

where $\rho = z/R$. The agreement between the calculated data and the analytical function is excellent. The other curves represent MC-calculated $G_0(z)$ for spheres with $R = 50$, but with radial density profiles following a hyperbolic form $\rho(r) = r^{-1}$. The density profile has a pronounced effect on the appearance of the $G_0(z)$ curves and also on the total scattering probability $G(0)$. For the full sphere, one has $\bar{r} = 3R/2 = 75$, whereas for $\rho(r) = r^{-1}$, the calculations gave $\bar{r} = 54$.

Figure 3 shows the MC-calculated $G_0(z)$ for hollow spheres with outer radius $R = 50$ and varying inner radii. Comparing $G_0(z)$ of the hollow spheres with that of the full sphere, the interesting feature is the appearance of a small shoulder at a z -value corresponding to the inner diameter of the hollow spheres.

$G_0(z)$ for core-shell spheres with inner radius $R_1 = 30$ and outer radius $R_2 = 50$ are plotted in Figure 4 for different combinations of the scattering length densities ρ_1 and ρ_2 . Some values of $\rho_1; \rho_2$ give rise to strong oscillations in $G_0(z)$, which were also found in the multishell calculations by Rekveld et al.

McTear 2000. The quantitative interpretation of these oscillations was given by Uca [?]. Minima arise from correlations between particle regions with opposite signs of their scattering length densities. Correspondingly, maxima are related to identical signs in different regions, or to correlations within the same region. The positions of these extrema give information on the typical distances between or within these regions. Thus, the position of minimum at $z = 40$ in Figure 4 is related to the typical shell-core distance, which is taken as the core radius plus half the shell thickness, which in the case shown in the Figure is exactly $R_1 + (R_2 - R_1)/2 = 40$. The maximum at $z = 70$ is due to the shell-shell correlations, of which the typical distance, taken as the core diameter plus twice the half shell thickness, is 80. The core-core correlations are expected to give a maximum around $z = R_1 = 30$, but this is hidden by the initial part of $G_0(z)$.

Alternatively, oscillations in $G_0(z)$ can be interpreted in terms of the differential parameters introduced in Section 3.2. Inserting the expansion (16) into (7) shows that each term in (16), except the zero-order term a_0 , produces a contribution to $G_0(z)$ containing a maximum. The position of such a maximum is shifted to higher z for higher order terms. Thus the minimum of $G_0(z)$ at $z = 40$ in Figure 4 can be attributed to a large negative differential parameter of high order in the expansion (16). Accordingly, the maximum at $z = 70$ comes from a positive differential parameter of even higher order. Relating such high-order differential parameters directly to structural features of the particle in a unique way is, however, a challenging task in small-angle scattering theory [?, ?, ?].

MC-calculated $G_0(z)$ for homogeneous and hollow cylinders are plotted in Figure 5. It should be noted that for cylinders with a high aspect ratio $L=2R$, the maximum of $p(r)$ is shifted towards small r . As a consequence, the least-squares method for determining $p(r)$ described in Section 3.2 must use a small number of data points. However, this is not found to pose a serious problem. The $G_0(z)$ curve for the homogeneous cylinder shows the same characteristic features as in the model calculations by Uca et al. Uca 2003. For the hollow cylinder, however, there are remarkable differences. The SESANS functions are concave at small z , and there is a clear shoulder at a position corresponding to the inner diameter. For the thinnest of the cylindrical shells, the shoulder appears to give a discontinuous first derivative at $z = 100$. In the corresponding $p(r)$ curve, the maximum also appeared discontinuous. Because of this, it was necessary to increase the accuracy of the numerical quadrature described in Section 3.3 to avoid numerical artefacts. At the highest z -values, the curves practically coincide, all showing the loss of correlations characteristic for anisotropic structures.

SESANS functions for core-shell cylinders analogous to the core shell spheres in Figure 4 are plotted in Figure 6. The inner and outer radii are $R_1 = 30$ and $R_2 = 50$, and the cylinder length is $L = 250$. The positions of minima and maxima can be interpreted in the same way as for the spheres. For the lowest curve, the correlations are almost completely lost already at $z = 100$. This can be related to the fact that for this particular combination of core and shell volumes and scattering length densities, the overall scattering length densities of the core and shell are nearly equal, but of different signs. Thus for z greater than 100, corresponding to correlations only along the cylinder axis, the core

and shell contributions cancel each other out.

In Figure 7 the SESANS functions for various triaxial ellipsoids are shown. The case for ellipsoids of revolution have been discussed by Uca et al. Uca2003. The SESANS functions of the ellipsoids with small eccentricities have been calculated by sampling points from a circumscribing sphere. For higher eccentricities, a circumscribing cylinder was used. Sampling random points from a confocal ellipsoidal coordinate system [?] would in principle eliminate the problem of sampling and discarding points that fall outside the ellipsoid. However, applying the inversion method of Appendix A to such special coordinate systems would in most cases require the numerical solution of nonlinear equations, thus losing the advantage of sampling efficiency.

We close this section with a discussion of the efficiency of the Monte Carlo method, with the prospective application of analyzing real SESANS data. The calculations in this work were performed using the random number generation ran3 given by Press et al. Numerical Recipes. This is a very reliable routine, but for the purpose of rapid calculations, simpler generators could be applied. Although the Monte Carlo method is general, the examples shown are for relatively simple structures. Additional refinements are possible, but to the cost of increased computing time. Polydispersity would require multiple calculations of

$\langle r \rangle$, as given by Equation (10) and (11), but this would in principle be required to be done only once for each $G_0(z)$ -spectrum. The presence of radial density profiles $\rho(r)$ could be included already in the Monte Carlo sampling procedure, as described in Appendix A. For a sphere, this method requires that $r^2 \rho(r)$ is described by an analytically invertible function. If not, an additional sampling must be performed, preferably from a distribution that closely follows $\rho(r)$, to obtain the desired density distribution. A gain, this calculation needs to be done only once for each $\rho(r)$.

5 Conclusion

Knowledge of analytical expressions for the SESANS correlation function $G_0(z)$ for a host of geometries and structures would be ideal and efficient for calculating model curves and analyzing experimental SESANS data. As such expressions are hard to obtain for complex structures due to the difficulty of deriving general expressions for $\rho(r)$ to be used in equation (7), one has had to apply the scattering functions from conventional small-angle scattering to equation (2) obtain $G_0(z)$. The Monte Carlo algorithm outlined in this paper represents an alternative method, which is general and straightforward to implement from the shape function of the geometry in question. The method does not need any of the special functions that frequently comes with the SANS scattering functions contained in $(d)=d$.

A Uniform sampling by the inversion method

Standard random number generators provide the user with random real numbers uniformly distributed between 0 and 1 [?]. Wishing to sample from a distribution function $f(x)$ defined on or limited to the interval $a \leq x \leq b$, one sets $f(x)(dx) = (d)$ and integrates, getting the following relation between the cumulative distribution $F(x)$ and the random variable ξ :

$$F(x) = \frac{\int_a^x f(x^0)(dx^0)}{\int_a^b f(x^0)(dx^0)} = \xi \quad (19)$$

Solving the inverse equation $x = F^{-1}(\xi)$, one can convert the random variable $0 < \xi < 1$ to random variables x uniformly distributed in $f(x)$.

Considering a sphere with radius R , the three spherical coordinates $r; \theta; \phi$ have the probability distributions $3r^2=R^3, 1=2, \frac{1}{2} \sin \theta$, respectively. A three-dimensional uniformly distributed random variable is then converted points uniformly distributed throughout the volume of the sphere by

$$\begin{aligned} r &= R \xi_1^{1/3} \\ \theta &= 2 \xi_2 \\ \cos \phi &= 1 - 2 \xi_3 \end{aligned} \quad (20)$$

When the geometry in question is, say, a hemisphere, a spherical sector or a spherical shell defined by the coordinates $(R_1; \theta_1; \phi_1)$ and $(R_2; \theta_2; \phi_2)$, the distribution functions can be limited to these regions. Equation (20) then generalizes to

$$\begin{aligned} r &= \sqrt[3]{\xi_1 R_2^3 - R_1^3} \\ \theta &= 2(\xi_2 - \xi_1) + \theta_1 \\ \cos \phi &= \cos \phi_1 - 3(\xi_3 - \xi_1)(\cos \phi_1 - \cos \phi_2) \end{aligned} \quad (21)$$

A further generalization is the inclusion of a radial distribution of scattering length by a function $\rho(r)$. Taking the function $\rho(r) = r^{-3}$, where $\xi < 3$, which in particular applies to spherical star polymers and polymeric micelles [?], the radial coordinate r follows the probability distribution $4r^2 \rho(r) = V = (3 - \xi)r^2 = R^3$, yielding in the case of a hollow sphere

$$r = \sqrt[3]{\xi R_2^3 - R_1^3} \quad (22)$$

In the case of a cylinder with radius R and length L , the coordinates $r; \theta; z$ follow the respective distributions $2r=R^2; 1=2; 1=L$, giving the relations:

$$\begin{aligned} r &= R \xi_1^{1/2} \\ \theta &= 2 \xi_2 \\ z &= \xi_3 L \end{aligned} \quad (23)$$

The corresponding generalizations to a cylindrical subvolume are:

$$\begin{aligned} r &= \sqrt{\xi_1 R_2^2 - R_1^2} \\ \theta &= 2(\xi_2 - \xi_1) + \theta_1 \\ z &= \xi_3 (L_2 - L_1) + L_1 \end{aligned} \quad (24)$$

For a rectangular box defined by a lower corner $(a_1; a_2; a_3)$ and an upper corner $(b_1; b_2; b_3)$, the transformation relations for the cartesian coordinates $(x_1; x_2; x_3)$ takes the simple form

$$x_i = (b_i - a_i) \xi_i + a_i: \quad (25)$$

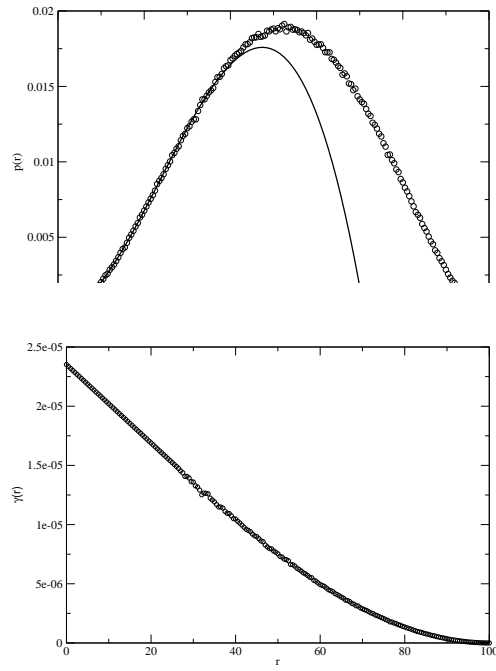


Figure 1: Right: Monte Carlo calculated pair distance distribution function $p(r)$ for a homogeneous sphere with radius $R = 50$. The solid line represents the polynomial $r^2 + a + br + cr^2$ that has been fitted to $p(r)$ up to $r = 26.5$. Left: density correlation function $\gamma(r)$ calculated from the $p(r)$ curve. The low- r part is calculated from the polynomial fit.

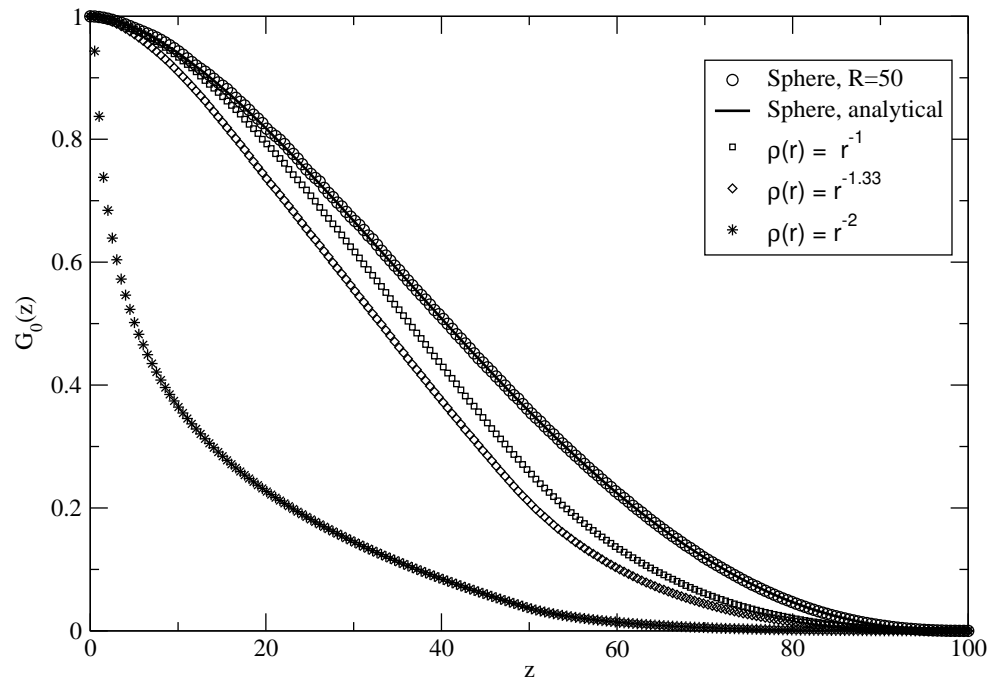


Figure 2: Monte Carlo calculated SESANS correlation function $G_0(z)$ for a homogeneous sphere with radius $R = 50$ (circles). The solid line represents the analytical expression for $G_0(z)$. The other curves represent spherical particles with a radial density distribution $\rho(r) = r^{-\alpha}$ and a maximum radius $R = 50$.

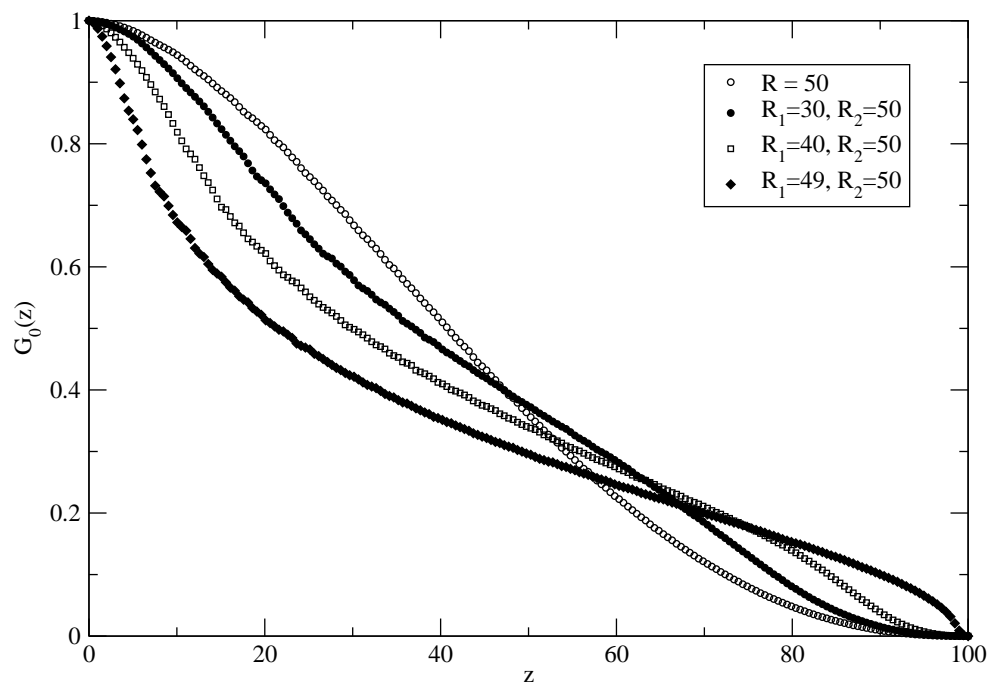


Figure 3: Monte Carlo calculated SESANS correlation functions for one homogeneous (open circles) and various hollow spheres.

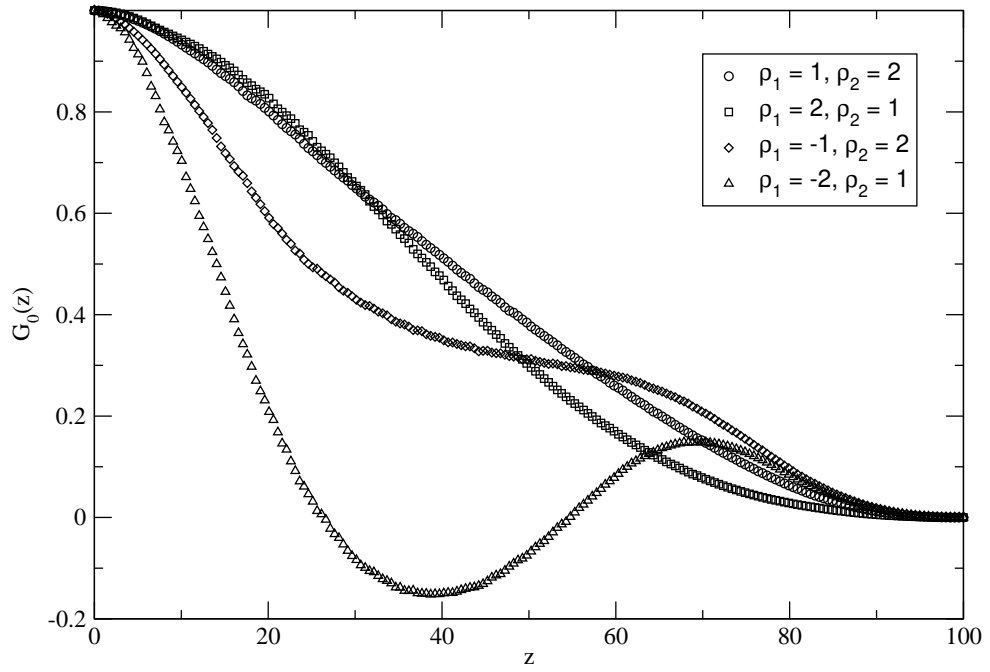


Figure 4: Monte Carlo calculated SE SANS correlation functions for a core-shell sphere with inner radius $R_1 = 30$ and outer radius $R_2 = 50$ with different scattering length densities.

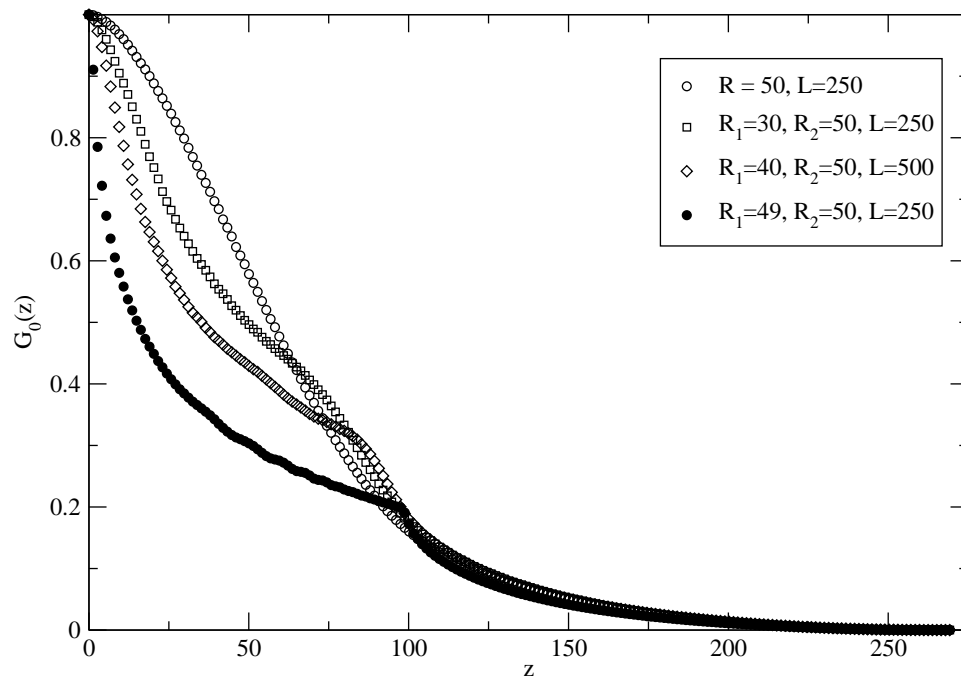


Figure 5: Monte Carlo calculated SESANS correlation functions for one homogenous and several hollow cylinders with outer radius $R_2 = 50$, different inner radii R_1 , and length $L = 250$.

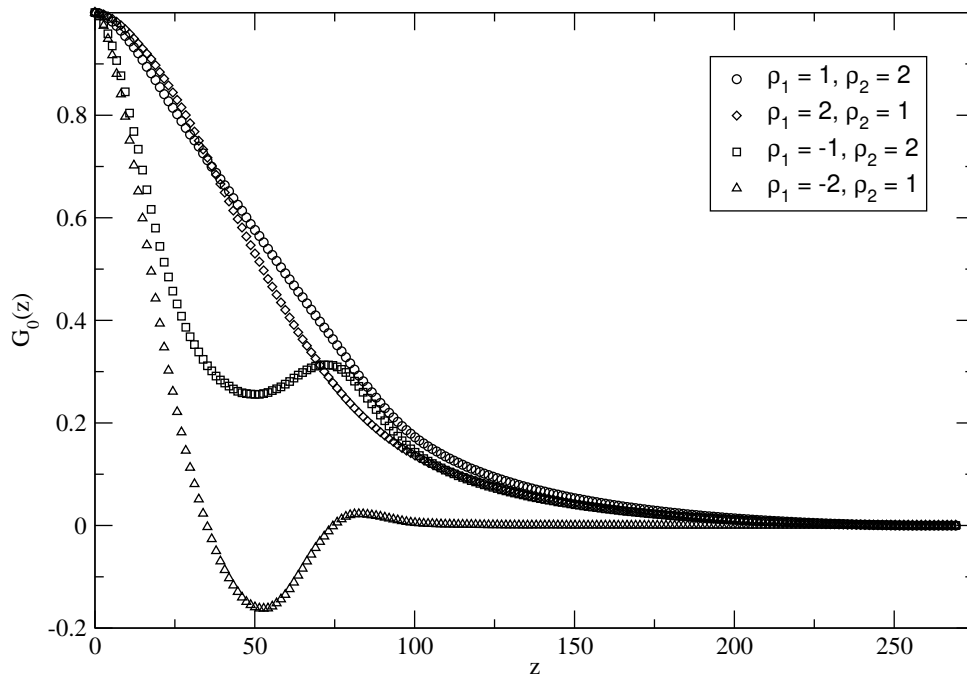


Figure 6: Monte Carlo calculated SE SANS correlation functions for a core-shell cylinder with inner radius $R_1 = 30$, outer radius $R_2 = 50$, and length $L = 250$ with different scattering length densities.

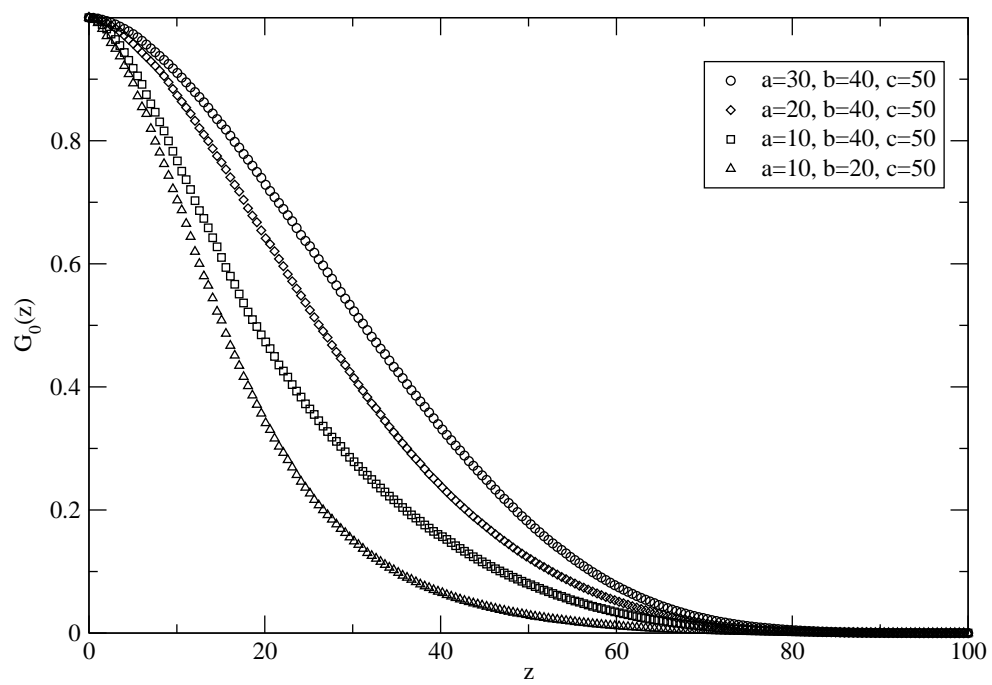


Figure 7: Monte Carlo calculated SESANS correlation functions for various triaxial ellipsoids.